Determination of the Local Cross-Link Density in Polyisobutylene-Based Elastomers by NMR Imaging

ARTICLE *in* MACROMOLECULES · JANUARY 2003

Impact Factor: 5.8 · DOI: 10.1021/ma021426w

4 AUTHORS, INCLUDING:

Peter Adriaensens
Hasselt University
261 PUBLICATIONS **2,232** CITATIONS
SEE PROFILE

Mauritz Kelchtermans
exxonmobil chemical europe
9 PUBLICATIONS **102** CITATIONS
SEE PROFILE

Determination of the Local Cross-Link Density in Polyisobutylene-Based Elastomers by NMR Imaging

Peter Adriaensens,[†] Anne Pollaris,[†] Mauritz Kelchtermans,[‡] and Jan Gelan*[,†]

Department SBG, Institute for Materialresearch (IMO), Limburg University, Universitaire Campus, B-3590 Diepenbeek, Belgium, and ExxonMobil Chemical Europe, Hermeslaan 2, B-1831 Machelen, Belgium

Received September 3, 2002; Revised Manuscript Received November 9, 2002

ABSTRACT: Gravimetrical Flory−Rehner experiments are combined with MRI experiments to study the spatially dependent degree of cross-linking in unfilled, 1,6-hexamethylenediamine-cured poly(isobutylene−*p*-methylstyrene−*p*-bromomethylstyrene) terpolymers. MRI relaxometry reveals two proton T_2 relaxation decay times in CCl_4 swollen specimens: a fast decaying component reflecting the constrained chain segments near cross-links and entanglements and a slow decaying component originating from less constrained, remote chains. On the basis of a linear relation between the bulk $M_{n,eff}$ (number-average molecular weight between effective cross-links) and the volume-averaged T_2 decay times, MRI allows the determination of the local cross-link density in inhomogeneously cross-linked specimens by means of the spatially dependent T_2 decay times. MRI solvent diffusion experiments reveal that the ingress kinetics of cyclohexane in PIB terpolymers is Fickian. It is shown that the diffusion coefficient varies linearly with the cure state and the volume-averaged T_2 decay times.

Introduction

Since its introduction by Lauterbur in 1973,[1] magnetic resonance imaging (MRI) has been developed into a modern approach for mapping the spatial morphology of elastomers. It is a unique, nondestructive, and noninvasive technique for the three-dimensional analysis of rubbery materials as demonstrated by the number of thorough reviews already published concerning cross-linking and aging of elastomers.[2−14]

The poly(isobutylene−*p*-methylstyrene−*p*-bromomethylstyrene) (PIB−PMS/BrPMS) is a promising second-generation butyl rubber because the gas-barrier properties of regular butyl rubber are maintained, while the resistance to oxidative degradation is enhanced due to the saturated polymer backbone.[15,16] As a consequence of the steric constraints associated with the methyl group packing,[17,18] the chain dynamics for polyisobutylene are significantly reduced as compared to other elastomers. This results in a short proton T_2 relaxation decay time (about 100 μs at room temperature), which consequently does not allow imaging isobutylene-based elastomers using the conventional MRI approach. As such, MRI data of polyisobutylene-based elastomers are noticeably absent in the literature. Swelling of these elastomers in an appropriate solvent enhances the molecular chain mobility and reduces the proton line width to an extent acceptable for MRI. This allows visualization of the morphology of well-defined features such as voids and cross-link density gradients.

In a previous paper,[14] it was shown that by swelling the elastomers in the aprotic solvent CCl_4, the proton signal in the MRI images originates almost exclusively from the rubber methyl protons. This makes it possible to acquire selective images of the rubbery phase, which were demonstrated to be superior toward the visualization of the network homogeneity. Swelling in a protic solvent like cyclohexane, on the other hand, permits to record selective images of the ingressed solvent, which are superior toward the visualization of occluded voids. In a subsequent paper, a statistical void density analysis was presented by which a strong linear correlation was demonstrated between the average number of voids per volume unit and the mechanical performance: the higher the microvoid density, the more the premature failure behavior.[19]

In the present study, proton MRI is used to study the distribution of the cross-link density in unfilled polyisobutylene-based elastomers cured with 1,6-hexamethylenediamine. Local inhomogeneities in cross-link density might originate from insufficient mixing and thermal gradients during vulcanization and can have a dramatic influence on the mechanical properties and final material performance. The local cross-link density, which determines the molecular mobility of the chain segments, can be visualized on the basis of local variations in the contrast determined by the proton T_2 relaxation decay time. In the second part of this paper, the local diversity in cross-link density is correlated with the diffusion behavior of ingressing cyclohexane.

Experimental Section

Materials. The PIB−PMS/BrPMS terpolymer specimens (Scheme 1) contain 97−98 mol % PIB and 3−2% PMS of which 0.5−2% is brominated. As such, the molecular chain dynamics and relaxation properties are quite similar to neat polyisobutylene. The unfilled, 1,6-hexamethylenediamine-cured specimens 1 to 4 are taken from four different batches. The degree of cross-linking increases from specimen 1 to specimen 4. Cross-linking occurs by a nucleophilic substitution reaction at the benzylic carbon by the diamine curative.[18]

Flory−Rehner Gravimetrical Experiments. Equilibrium swelling in cyclohexane was performed at ambient temperature. The bulk number-average molecular weight between

[†] Limburg University.
[‡] ExxonMobil Chemical Europe.
* To whom correspondence should be addressed: Tel ++32(0)-11 26 83 88; Fax: ++32(0)11 26 83 01; e-mail jan.gelan@luc.ac.be.

10.1021/ma021426w CCC: $25.00
Published on Web 01/14/2003

Scheme 1. Chemical Structure of the PIB−PMS/BrPMS Terpolymer

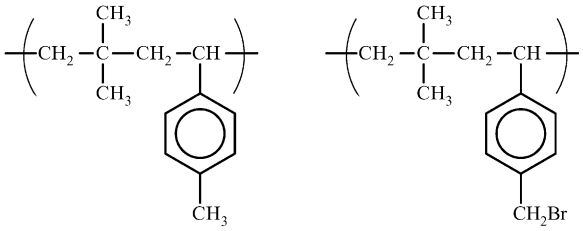

effective cross-links was derived from the Flory−Rehner equation:[8,20]

$$1/M^{b}_{n,eff} = \frac{-[\ln(1 - V_r) + V_r + \chi V_r^2]}{\rho_r V_0 (V_r^{1/3} - V_r/2)} \quad (1)$$

in which χ is the Flory−Huggins polymer−solvent interaction parameter, ρ_r the density of the unswollen rubber, being 0.917 g/cm^3, and V_0 the molar volume of the swelling solvent, being 108 cm^3/mol. The value of V_r, being the volume fraction of rubber in the swollen vulcanizate, was determined by means of eq 2:

$$V_r = \left[\left(\frac{\rho_r}{\rho_s}\right)\left(\frac{W_\infty - W_0}{W_0}\right) + 1\right]^{-1} \quad (2)$$

in which ρ_s is the solvent density, being 0.779 g/cm^3, W_∞ the equilibrium weight of the swollen rubber, and W_0 the initial weight of the unswollen rubber sample. The Flory−Huggins interaction parameter χ, being concentration dependent, is obtained from the following power series (eq 3):

$$\chi = \chi_0 + \chi_1 V_r + \chi_2 V_r^2 \quad (3)$$

with $\chi_0 = 0.44$, $\chi_1 = -0.083$, and $\chi_2 = 0.068$ for the system PIB−cyclohexane.[21]

MRI. All MRI images were acquired at room temperature on a Varian Inova 300 vertical bore spectrometer equipped with an actively shielded imaging probe having an inner diameter of 25 mm. To further reduce B_1 field inhomogeneities, a maximum sample diameter of 20 mm was used. Rubber images were obtained after swelling to equilibrium in CCl_4 and have an in-plane pixel resolution of 100 × 100 μm, a slice thickness of 2 mm, and a field of view (FOV) of 25 × 25 mm. For each specimen, the volume-averaged proton T_1 relaxation decay time was determined by fitting the 1-D projection signal intensity vs a variable repetition delay TR according to eq 4. The volume-averaged proton T_2 relaxation behavior was obtained by analyzing the intensity of 1-D projections, obtained as a function of the echo time TE according to the following biexponential equation (eq 5):

$$M_t = M_0[1 - \exp(-TR/T_1)] \quad (4)$$

$$M_t = M_{0,s}\exp(-TE/T_{2,s}) + M_{0,l}\exp(-TE/T_{2,l}) \quad (5)$$

in which $M_{0,s}$ and $T_{2,s}$ represent the fraction and time constant of the constrained network chains closely around the cross-links, while $M_{0,l}$ and $T_{2,l}$ represent the fraction and time constant of the more mobile chains. To determine the local T_2 relaxation decay times, rubber images were recorded as a function of TE (TE values between 7.2 and 200 ms) with a classical spin-warp pulse sequence[22] and a fixed (equilibrium) repetition delay TR of 1 s. Regions of interest were only selected in the inner part of the specimens where the B_1 field is highly homogeneous.

Diffusion Kinetics. To study the diffusion kinetics of cyclohexane ingress, MRI images with a slice thickness of 0.75 mm, a TE = 16 ms, and a TR = 0.5 s were recorded as a function of time. For this purpose, cylindrical samples with a diameter of 9.5 mm and a height of 2 mm were cut and immersed in cyclohexane at ambient temperature. A Teflon stopper was placed on top of the cylinder to avoid longitudinal solvent ingress. The surrounding free solvent can be easily differentiated from the ingressed solvent due to its different T_1 decay time (dark gray outer region in Figure 5). During the polymer swelling, MRI makes it possible to measure the diffusion distance based on the following equation (eq 6):[23]

$$\text{diffusion distance} = \frac{\text{original diameter} - \text{diameter core}}{2} \quad (6)$$

The calculation of the surface of the central unswollen core, from which the mean core diameter was derived, was performed on a Macintosh computer using the public domain NIH Image program (developed at the U.S. National Institutes of Health).

The diffusion kinetics were determined by the time dependency of the diffusion distance according to eq 7:[24]

$$\log(\text{diffusion distance}) \sim n \log(\text{time}) \quad (7)$$

in which n theoretically lies between 0.5 for pure Fickian diffusion and 1.0 for pure case II diffusion. In the case of Fickian diffusion, the diffusion coefficient D can be determined by plotting the diffusion distance d as a function of square root of time according to eq 8:[24]

$$d = \sqrt{2D}\sqrt{t} \quad (8)$$

Results and Discussion

Determination of the Bulk Cross-Link Density and Volume-Averaged T_2 Decay Times. Although NMR imaging allows the visualization of inhomogeneities at a mesoscopic level (tens of micrometers), its strength is mainly situated in the ability to probe the underlying dynamical events at the nanometer level via relaxometry. As was already demonstrated in a preceding paper, selective MRI images of the rubber proton spins, obtained after swelling in a nonprotonated solvent, can be employed to visualize the homogeneity of the cross-link density.[14] Regions of low proton signal intensity correspond to environments in which the segmental chain dynamics is strongly constrained by cross-links (short T_2 decay time), while regions of high proton signal intensity correspond to chain segments in low cross-link density areas (long T_2 decay time). A typical example is presented in Figure 1, showing the "rubber" images of PIB−PMS/BrPMS elastomers, which are cured to different cure states, after swelling in CCl_4. This first part of the paper deals with the determination of the bulk cross-link density of these specimens by means of the Flory−Rehner method and its correlation with the volume-averaged T_2 relaxation decay times. This relation forms the basis for the determination of the spatially dependent cross-link densities.

For the different cure states, the bulk number-average molecular weight between the effective cross-links ($M^{b}_{n,eff}$), as determined by gravimetrical Flory−Rehner experiments in cyclohexane (eqs 1−3), is presented in Table 1. In Figure 2, a nice inverse linear correlation (correlation coefficient $R = 0.968$) is demonstrated between the bulk $M^{b}_{n,eff}$ and the torque values obtained with a mechanical oscillating disk rheometer.[10] The higher the cross-link density, resulting in a higher torque, the lower the number-average molecular weight between the effective cross-links. These gravimetrical results confirm the presence of an appreciable variation in the bulk cross-link density for the different

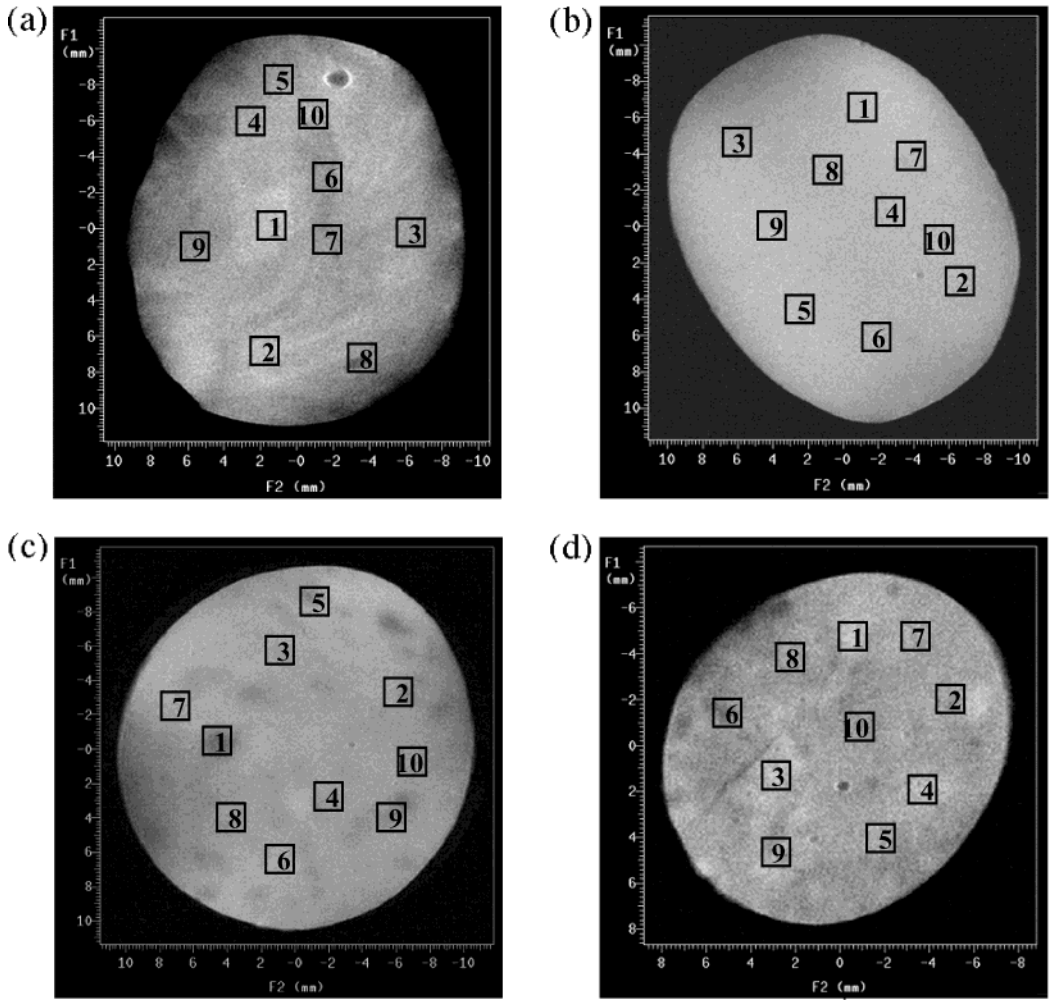

Figure 1. MRI rubber images of unfilled PIB-based terpolymers, cured with 1,6-hexamethylenediamine, after equilibrium swelling in CCl_4: (a) specimen 1, (b) specimen 2, (c) specimen 3, and (d) specimen 4. The specimens result from four different batches and have an increasing degree of cure. The ROI's indicate the locations used to determine the local relaxation decay times.

Table 1. Gravimetrical Results Obtained for the Unfilled 1,6-Hexamethylenediamine-Cured PIB Terpolymers (Equilibrium Swelling in C_6H_{12})[a]

	V_r	bulk $M^b_{n,eff}$	torque (dN m)
specimen 1	8.45×10^{-2}	56 954	4.4
specimen 2	8.75×10^{-2}	52 821	9.1
specimen 3	11.95×10^{-2}	26 641	14.9
specimen 4	20.58×10^{-2}	7 337	28.8

[a] The cure state enhances from specimen 1 toward specimen 4 as is demonstrated by the torque values of the rheological experiments.

elastomer specimens as was already demonstrated by the rheological experiments.

Table 2 shows the volume-averaged proton T_1 and T_2 relaxation decay times after equilibrium swelling in CCl_4. While the T_1 decays are monoexponential (eq 4), the T_2 analysis (eq 5) results in a short ($T_{2,s}$) and a long decay time ($T_{2,l}$). The short T_2 fraction can be assigned to the network chain segments that are constrained by surrounding cross-links and entanglements, while the long T_2 fraction represents mobile network chains, more remote from the cross-links and entanglements.[9,25] The molar fraction weighted volume-averaged T_2 decay time ($T_{2,mfw}$) is also presented in Table 2.

From Table 2 it is clear that, in contrast to the (comparable) T_1 decay times, the T_2 decay times are clearly dependent on the degree of cross-linking of the

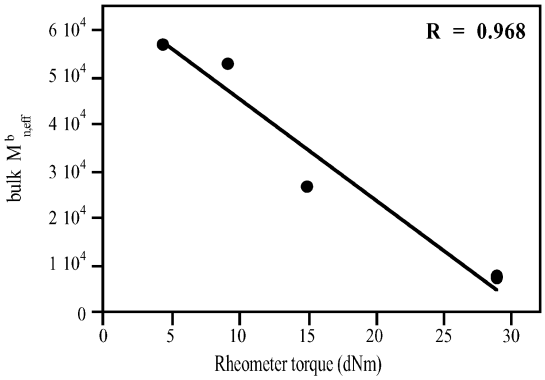

Figure 2. Bulk number-average molecular weight between the effective cross-links ($M^b_{n,eff}$) as a function of rheometer torque (R = correlation coefficient).

elastomer. The long component $T_{2,l}$, as well as $T_{2,s}$ and $T_{2,mfw}$ decrease with increasing degree of cross-linking. Indeed, as the efficiency of the T_2 relaxation is highly sensitive to low-frequency motions like these of the backbone chains, the average chain length between effective cross-links will strongly impact on the T_2 decay time. The relation between the bulk $M^b_{n,eff}$ and the volume-averaged T_2 decay times is presented in Figure 3: linear correlations are observed between the T_2 decay times (representing the molecular chain mobility) and

Table 2. Volume-Averaged T_1 and T_2 Relaxation Decay Times (and Fractions $M_{0,i}$) of the Unfilled 1,6-Hexamethylenediamine-Cured PIB Terpolymers, Swollen to Equilibrium in CCl_4

	bulk $M^b_{n,eff}$	T_1 (s)	$T_{2,s}$ (ms)	$M_{0,s}$ (%)	$T_{2,l}$ (ms)	$M_{0,l}$ (%)	$T_{2,mfw}$ (ms)[a]
specimen 1	56 954	0.18	15.4	32.1	86.3	67.9	63.6
specimen 2	52 821	0.17	15.0	28.4	70.8	71.6	54.9
specimen 3	26 641	0.18	8.8	41.9	48.7	58.1	32.0
specimen 4	7 337	0.17	5.78	65.7	23.8	34.3	12.0

[a] $T_{2,mfw}$ represents the molar fraction weighted volume-averaged T_2 decay time.

Table 3. Spatially Dependent T_2 Relaxation Decay Times and Cross-Link Densities ($M^l_{n,eff}$) for the Unfilled 1,6-Hexamethylenediamine-Cured PIB Terpolymers, Swollen to Equilibrium in CCl_4 (Mean and Standard Deviation Are Indicated)

	specimen 1		specimen 2		specimen 3		specimen 4	
	$T^l_{2,mfw}$ (ms)	$M^l_{n,eff}$	$T^l_{2,mfw}$ (ms)	$M^l_{n,eff}$	$T^l_{2,mfw}$ (ms)	$M^l_{n,eff}$	$T^l_{2,mfw}$ (ms)	$M^l_{n,eff}$
spot 1	99.2	94 839	63.5	58 906	27.1	22 379	13.7	8899
spot 2	62.0	57 462	56.7	52 137	37.7	33 034	11.8	7045
spot 3	71.4	66 917	55.4	50 804	35.6	30 932	14.0	9239
spot 4	90.1	85 640	53.8	49 153	33.9	29 255	13.7	8876
spot 5	58.1	53 557	56.2	51 564	29.1	24 356	12.7	7861
spot 6	63.8	59 210	60.4	55 849	43.0	38 364	10.9	6077
spot 7	58.8	54 179	44.3	39 624	41.2	36 570	13.2	8377
spot 8	37.1	32 375	58.8	54 257	37.1	32 381	11.4	6609
spot 9	60.4	55 796	59.6	55 039	32.1	27 437	12.5	7737
spot 10	46.1	41 504	57.0	52 455	34.0	29 305	12.3	7550
mean ± std dev (%)		60 148 ± 31.0		51 979 ± 9.9		30 401 ± 16.4		7827 ± 13.3

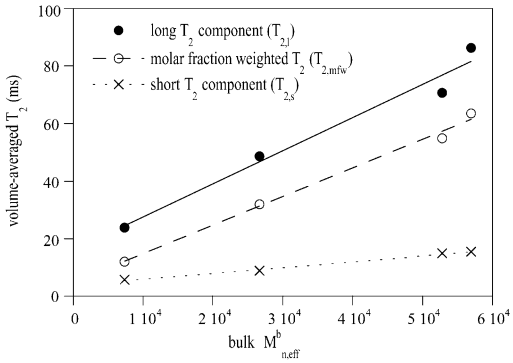

Figure 3. Volume-averaged T_2 relaxation decay times as a function of the bulk cross-link density ($M^b_{n,eff}$).

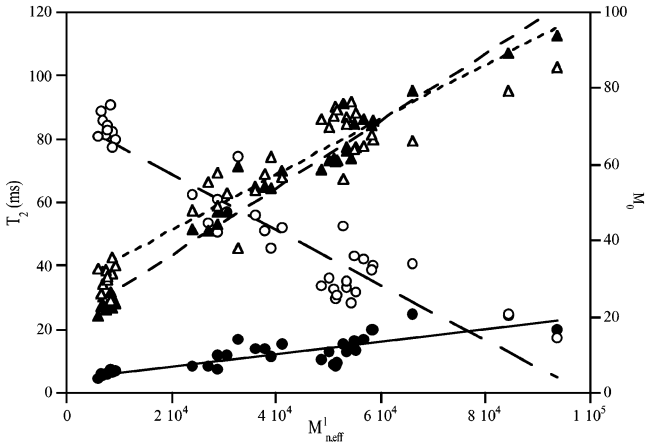

Figure 4. Spatially dependent T_2 decay times ($T_{2,s}$: ● and $T_{2,l}$: ▲) and their relative fractions ($M_{0,s}$: ○ and $M_{0,l}$: △) of the ROI's presented in Figure 1 of all four rubber specimens as a function of $M^l_{n,eff}$.

the bulk cross-link density $M^b_{n,eff}$ that can be expressed by the following equations (the correlation coefficient R for the curve fitting is indicated)

$$T_{2,l} = 16.10 + 11.49 \times 10^{-4} M^b_{n,eff} \quad (R = 0.986) \quad (9)$$

$$T_{2,mfw} = 4.83 + 9.95 \times 10^{-4} M^b_{n,eff} \quad (R = 0.997) \quad (10)$$

$$T_{2,s} = 3.96 + 2.02 \times 10^{-4} M^b_{n,eff} \quad (R = 0.996) \quad (11)$$

of which mainly $T_{2,l}$ and $T_{2,mfw}$ are strongly dependent on the bulk $M^b_{n,eff}$.

Determination of the Spatially Dependent T_2 Decay Times and Cross-Link Densities. These equations can further be used to trace the localized and spatially dependent degree of cross-linking. Therefore, the localized T_2 decay times were determined for the regions of interest (ROI's) displayed in Figure 1. This allows deducing the localized molecular weight between the effective cross-links ($M^l_{n,eff}$) for each ROI. Table 3 presents the results based on the spatially dependent, molar fraction weighted T_2 values ($T^l_{2,mfw}$) for the different rubber specimens.

Specimen 1 (Figure 1a) clearly exposes a very heterogeneous network structure as is also illustrated by a large variation in the localized $M^l_{n,eff}$ (Table 3), indicating an unfavorable mixing. This in strong contrast to specimen 2, having a rather homogeneous network structure as is demonstrated by the small variation in $M^l_{n,eff}$. This information supports a good, homogeneous mixing, resulting in a uniform curing. The homogeneity of mixing of the two remaining elastomers (specimens 3 and 4) is somewhere in between. Table 3 also demonstrates that the mean value of $M^l_{n,eff}$ closely approaches the values obtained by gravimetry (Table 2).

The complete set of results of the spatially dependent T_2 analysis (decay times and fractions) as a function of $M^l_{n,eff}$ is graphically displayed in Figure 4. The short decaying component, $T_{2,s}$, increases only slightly with decreasing cross-link density since it represents chain segments around the cross-links. Its fraction of course is strongly reduced upon lowering the degree of cross-linking. The long T_2 component ($T_{2,l}$), as well as its fraction ($M_{0,l}$), clearly increase with decreasing cross-link density.

Solvent Diffusion Experiments. Polymers are in many different applications exposed to solvents, which

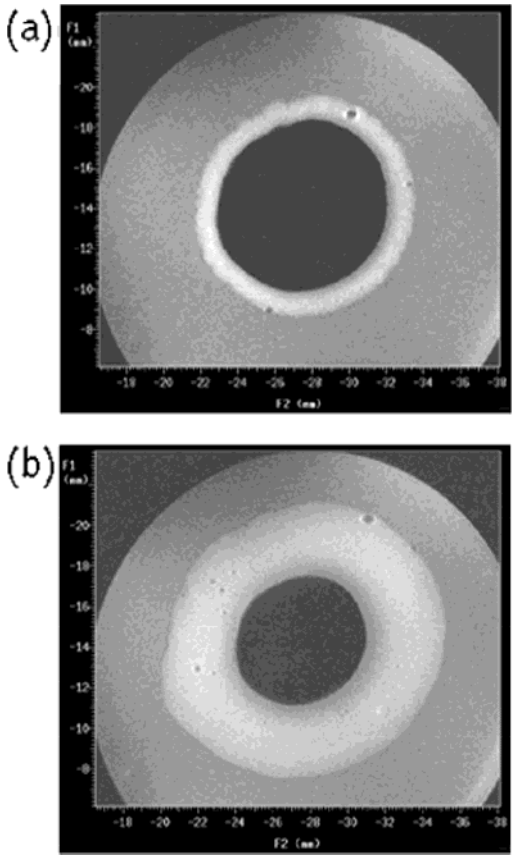

Figure 5. MRI images of the diffusion of cyclohexane in specimen 2 as a function of time: (a) after 45 min, (b) after 6 h 16 min.

can have a deteriorating effect on their mechanical properties such as tensile strength and fatigue resistance. Evaluation of the diffusion kinetics for a given polymer/solvent system can provide important physicochemical information.[12] MRI has been established as an excellent method to monitor the diffusion of penetrants into polymers in a nondestructive and noninvasive manner.[26−29] One of the major advantages of MRI, as compared with weight gain measurements, is the ability to separate the diffusion process, being a molecular and hence a specimen-shape-independent process, from the matrix swelling, being a macroscopic and hence shape-dependent process. The next part deals with the use of MRI to study the diffusion kinetics of cyclohexane into the unfilled PIB terpolymers as a function of the cross-link density.

Figure 5 presents some solvent MRI images of the diffusion of cyclohexane in specimen 2 as a function of ingress time. Two different processes can clearly be discriminated: solvent penetration into the rod and polymer matrix swelling. The diffusion front of the ingressing solvent can easily be distinguished from the unswollen, inner core. By plotting the logarithm of the diffusion distance (eq 6) vs the logarithm of time (eq 7), a Fickian diffusion behavior is observed for all four specimens ($n \approx 0.5$)[24] (Table 4). Indeed, since the diffusion experiments are performed far above the T_g of polyisobutylene, the polymer is in the rubbery state, and the solvent ingress is under diffusion control (case I or Fickian) instead of under chain relaxation control (case II).[30,31] This permits to extract the diffusion coefficients (eq 8) of which the values are included in Table 4. The results in Table 4 already indicate a decreasing ingress rate with increasing cross-link density.

Table 4. Diffusion Kinetics Parameters *n* and *D* for the Diffusion of Cyclohexane in the Unfilled, 1,6-Hexamethylenediamine-Cured, PIB Specimens

	$M^{b}_{n,eff}$	$T_{2,mfw}$ (ms)[a]	n	D (cm^2/s)
specimen 1	56 954	63.56	0.56	5.29×10^{-7}
specimen 2	52 821	54.91	0.56	5.54×10^{-7}
specimen 3	26 641	31.98	0.52	3.76×10^{-7}
specimen 4	7 337	11.95	0.54	2.95×10^{-7}

[a] $T_{2,mfw}$ represents the molar fraction weighted volume-averaged T_2 decay time.

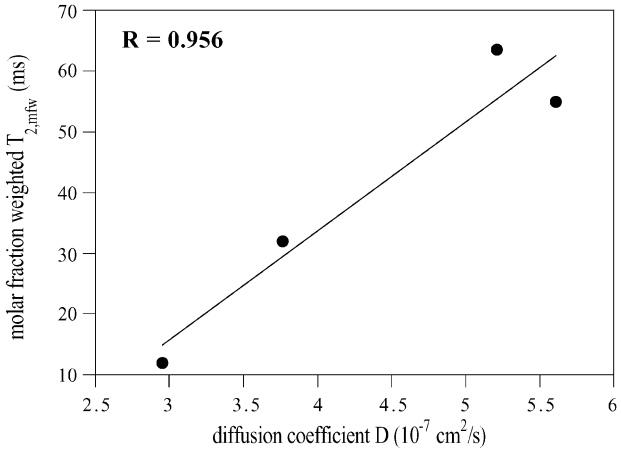

Figure 6. Plot of the volume-averaged molar fraction weighted T_2 relaxation time ($T_{2,mfw}$) as a function of the diffusion coefficient D (R = correlation coefficient).

The sorption behavior of rubbery polymers is controlled by the polymer structure, cross-link density, type of solvent, and temperature.[32] Since all diffusion experiments are performed on the same material (unfilled 1,6-hexamethylenediamine-cured, PIB terpolymers) at ambient temperature and with the same solvent (cyclohexane), the variation in the sorption behavior only depends on the difference in cure state of the specimens. Figure 6 shows a plot of the volume-averaged molar fraction weighted T_2 decay time ($T_{2,mfw}$) vs the diffusion coefficient D for the different specimens. From Table 4 and Figure 6, it is clear that the diffusion coefficient increases quasi-linearly with increasing $T_{2,mfw}$ or decreasing cure state (correlation coefficient $R = 0.956$), and this linear relation is expressed by eq 12.

$$T_{2,mfw} = -38.03 + 17.93 \times 10^{7} D \qquad (12)$$

This is in agreement with literature, where it is generally expected that the diffusion coefficient increases approximately linearly with decreasing cross-link density for noncrystalline polymers.[33,34] This even seems to be the case for rather inhomogeneous specimen as studied in this paper. On the other hand, the diffusion coefficient obtained for specimen 1 is somewhat smaller as was expected on the basis of the volume-averaged $T_{2,mfw}$, probably due to the unfavorable mixing that results in a rather pronounced heterogeneous network structure (Figure 1, Table 3). The strength of MRI lies in the possibility to visualize these inhomogeneities. Furthermore, the linear relation between the bulk $T_{2,mfw}$ and the diffusion coefficient (Figure 6 and eq 12) can also be used to estimate the spatially

dependent values of the diffusion coefficient in inhomogeneous specimens based on the local $T^{l}_{2,mfw}$ decay times presented in Table 3 (results not shown).

Conclusions

The results presented in this paper clearly demonstrate that MRI is a useful technique to study the homogeneity of mixing and consequently curing of (PIB-based) elastomers. The importance of homogeneous mixing procedures with respect to the final mechanical properties needs no further comment. Combined with complementary gravimetrical data from macroscopic swelling experiments (Flory−Rehner), MRI offers detailed information about the dynamical behavior of the rubber chain segments at the molecular level. Although NMR imaging allows the visualization of inhomogeneities at a mesoscopic level (tens of micrometers), its strength is mainly situated in the ability to probe the underlying dynamical events at the nanometer level via T_2 relaxometry. More specific, on the basis of the linear relation between the bulk T_2 decay times and the bulk degree of cross-linking, the spatially dependent T_2 decay times make it possible to determine the local $M^{l}_{n,eff}$ in inhomogeneously mixed (and/or cured) elastomers. MRI further allows determining the local diffusion coefficient in such specimens based on the linear relation between the T_2 decay times and the diffusion coefficient.

Acknowledgment. The authors acknowledge ExxonMobil Chemical for the financial support of this work. This research fits in the framework of the IUAP (Belgian Program on Interuniversity Attraction Poles, financed by the Belgian Government).

References and Notes

(1) Lauterbur, P. *Nature (London)* **1973**, *242*, 190.
(2) Blümich, B.; Blümler, P.; Gasper, L.; Guthausen, A.; Gobbels, V.; Laukemper-Ostendorf, S.; Unseld, K.; Zimmer, G. *Macromol. Symp.* **1999**, *141*, 83.
(3) Koenig, J. L. *Rubber Chem. Technol.* **2000**, *73*, 385.
(4) Demco, D. E.; Blümich, B. *Curr. Opin. Solid State Mater.* **2001**, *5*, 195.
(5) Kuhn, W.; Klein, M.; Wiesmath, A.; Demco, D. E.; Blümich, B.; Kelm, J.; Gold, P. W. *Magn. Reson. Imag.* **2001**, *19*, 497.
(6) Blümler, P.; Blümich, B. *Rubber Chem. Technol.* **1997**, *70*, 468.
(7) Sarkar, S. N.; Komoroski, R. A. *Macromolecules* **1992**, *25*, 1420.
(8) Schneider, M.; Demco, D. E.; Blümich, B. *Macromolecules* **2001**, *34*, 4019.
(9) Smith, S. R.; Koenig, J. L. *Macromolecules* **1991**, *24*, 3496.
(10) Oh, S. J.; Koenig, J. L. *Polymer* **1999**, *40*, 4703.
(11) Klei, B.; Koenig, J. L. *Acta Polym.* **1997**, *48*, 199.
(12) Gussoni, M.; Greco, F.; Mapelli, M.; Vezzoli, A.; Ranucci, E.; Ferruti, P.; Zetta, L. *Macromolecules* **2002**, *35*, 1722.
(13) Ercken, M.; Adriaensens, P.; Vanderzande, D.; Gelan, J. *Macromolecules* **1995**, *28*, 8541.
(14) Adriaensens, P.; Pollaris, A.; Vanderzande, D.; Gelan, J.; White, J. L.; Dias, A. J.; Kelchtermans, M. *Macromolecules* **1999**, *32*, 4692.
(15) Merrill, N. A.; Powers, K. W.; Wang, H. C. *Polym. Prepr.* **1992**, *33*, 962.
(16) Ashbaugh, J. R.; Ruff, C. R.; Shaffer, T. D. *J. Polym. Sci., Part A: Polym. Chem.* **2000**, *38*, 1680.
(17) Boyd, R. H.; Pant, P. V. K. *Macromolecules* **1991**, *24*, 6325.
(18) White, J. L.; Dias, A. J.; Ashbaugh, J. R. *Macromolecules* **1998**, *31*, 1880.
(19) Adriaensens, P.; Pollaris, A.; Vanderzande, D.; Gelan, J.; White, J. L.; Kelchtermans, M. *Macromolecules* **2000**, *33*, 7116.
(20) Flory, P. J. *J. Chem. Phys.* **1950**, *18*, 108.
(21) Brandrup, J.; Immergut, E. H. *Polymer Handbook*, 3rd ed.; John Wiley & Sons: New York, 1989.
(22) Kumar, A.; Welti, D.; Ernst, R. R. *J. Magn. Reson.* **1975**, *18*, 69.
(23) Ercken, M.; Adriaensens, P.; Reggers, G.; Carleer, R.; Vanderzande, D.; Gelan, J. *Macromolecules* **1996**, *29*, 5671.
(24) Webb, A. G.; Hall, L. D. *Polymer* **1991**, *32*, 2926.
(25) Fukumori, K.; Kurauchi, T.; Kamigaito, O. *Polymer* **1990**, *31*, 713.
(26) Ercken, M.; Adriaensens, P.; Vanderzande, D.; Gelan, J. *Macromolecules* **1995**, *28*, 8541.
(27) Weisenberger, L. A.; Koenig, J. L. *Appl. Spectrosc.* **1989**, *42*, 1117.
(28) Perry, K. L.; McDonald, P. J.; Clough, A. S. *Magn. Reson. Imag.* **1994**, *12*, 217.
(29) Laity, P. R.; Glover, P. M.; Barry, A.; Hay, J. N. *Polymer* **2001**, *42*, 7701.
(30) Alfrey, A.; Gurnee, E. F.; Lloyd, W. G. *J. Polym. Sci., Part C* **1966**, *12*, 249.
(31) Crank, J. *The Mathematics of Diffusion*, 2nd ed.; Clarendon Press: Oxford, 1975.
(32) Desai, S.; Thakore, I. M.; Devi, S. *Polym. Int.* **1998**, *47*, 172.
(33) Meares, P. *Polymers: Structure and Bulk Properties*; Van Nostrand: London, 1965.
(34) Unnikrishnan, G.; Thomas, S. *J. Polym. Sci., Part B: Polym. Phys.* **1997**, *35*, 725.

MA021426W